Effective Modes for a Strongly Coupled Quantum Emitter-MoS$_2$ Nanodisk System

Zhao-Shi Deng, Ling-Yan Li, Chun-Lian You, Yu-Wei Lu ⦿, and Jing-Feng Liu ⦿

Abstract—**We present an effective modes theory for studying the strong light-matter interaction and better understanding the non-Markovian dynamics of a quantum emitter (QE) coupled to two-dimensional materials. Specifically, we investigate the spontaneous emission of a V-type QE in close proximity to a MoS$_2$ nanodisk. The non-Markovian population dynamics is observed and found linked to the initial states, indicating that the coupled system enters the strong-coupling regime. The effective modes analysis shows that though a dozen of resonant modes appear in the photonic density of states, only a few modes have significant contribution to the population dynamics. Our work demonstrates the effective modes theory as a powerful tool to explore and optimize the quantum states control of QE by two-dimensional materials.**

Index Terms—**Quantum optics, light-matter interaction, quantum electrodynamics, nanodisk.**

I. INTRODUCTION

LOCALIZED surface plasmons supported by plasmonic nanostructures can dramatically alter the photonic density of states and cause a significant enhancement of the light-matter interaction [1], [2]. The enhanced light-matter interaction has potential applications ranging from nanoscale coherent light source [3], [4], biological nanoprobe [5], [6] to advanced quantum technologies, such as ultrasensitive quantum sensing [7]. Therefore, a lot of experimental and theoretical research works have been devoted to studying the strong coupling between the quantum emitters (QEs) and various metallic nanoparticles [8], [9], [10]. To achieve the strong coupling, QEs are often placed near the structures since light is confined in the sub-wavelength region around the metallic surface [11], [12], [13], [14], [15], [16], [17]. Besides the metallic nanoparticles, two-dimensional (2D) materials, such as graphene disk [18], [19], [20] and molybdenum disulfide nanodisk (MoS2) [21], [22], [23], [24], emerge as another promising platform for tuning light-matter interactions into the strong-coupling regime with the advantages

of *in situ* control and unprecedented degree of freedom [25], and demonstrating the compelling applications like the infrared photodetector [26] with extraordinary optoelectronic properties and integrated neuromorphic hardware [27].

Recently, extensive theoretical works have also been done to extend the cavity quantum electrodynamics (cQED) concept to study the strongly coupled plasmon-QE hybrid system at nanoscale, and demonstrated some interesting phenomena like the quantum interference effect due to the anisotropic Purcell effect of 2D materials [28], [29], [30], [31]. However, to the best of our knowledge, a simple and physically transparent picture of the coherent energy exchange between the QE and the 2D materials is still lacking, due to the broadband and non-Lorentzian Purcell factor. The complicated optical response of 2D materials leads to the failure in directly applying the cQED treatments into such hybrid systems, since the 2D materials cannot be considered as a conventional Lorentzian resonantor. The effective mode theory describes the plasmon-QE interaction in the language of cQED where the creation and annihilation operators no longer have a continuous spectral dependence. Instead, the complicated plasmonic response is reconstructed by a set of separated, lossy field operator associated with the respective resonance peaks of given structure. The connection between the effective modes and the original quantization is well defined, so that all the required parameters in the effective models can be easily obtained from the Green's tensor of the system [28], [29].

In this work, we study the population dynamics of a V-type QE strongly coupled to a MoS$_2$ nanodisk by developing an effective multi-mode approach, which can precisely approximate the complicated response of MoS$_2$ by a dozen of Lorentzian cavity modes. Subsequently, the quantum dynamics of the hybrid system is described by an effective model in full analogy with multi-mode Jaynes–Cummings Hamiltonian. We show that our method can successfully capture the non-Markovian dynamics of strongly coupled QE-MoS$_2$ system.

II. THEORY

The quantum system we study is depicted in Fig. 1, which consists of a V-type QE closely located to a MoS$_2$ nanodisk with radius R. The origin of the coordinate system is chosen at the center of nanodisk, and the plane of nanodisk lies in the xy plane. A QE with two degenerate excited states $|1\rangle$, $|2\rangle$ and one ground state $|0\rangle$ is located at distance z from the surface of nanodisk. The transition frequency between the two degenerate excited states and the ground state is characterized by ω_0, where
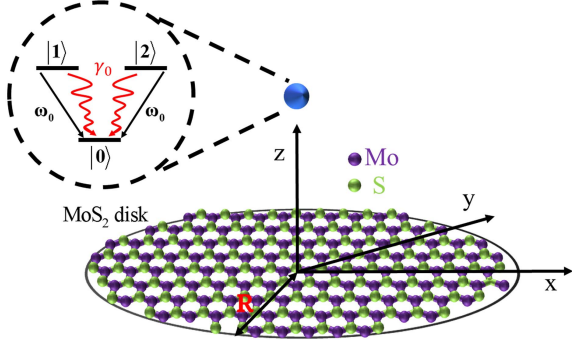
Fig. 1. Schematic of the hybrid system we study. The radius of MoS$_2$ nanodisk is $R = 30$ nm. A V-type QE with two degenerate excited states is placed at $\mathbf{r}_d = (0, 0, z)$. The transition frequency of two excited states of the V-tpe QE is characterized by ω_0, the decay rate of two excited states of the V-type QE is denoted as γ_0.

the energy of ground state $|0\rangle$ has been set to zero. The dipole moment can be written as $\mathbf{d}_{10} = d\mathbf{e}_-$ and $\mathbf{d}_{20} = d\mathbf{e}_+$, where $\mathbf{e}_\pm = (1/\sqrt{2})(\mathbf{e}_z \pm i\mathbf{e}_x)$ denotes the right- and left-rotating unit vectors, and d is taken as a real number [32].

The Hamiltonian of the system is given by

$$\hat{H} = \sum_{i=1,2} \hbar\left(\omega_0 - i\frac{\gamma_0}{2}\right)\hat{\sigma}_{ii} + \int d\mathbf{r} \int_0^{+\infty} d\omega \hbar\omega \hat{\mathbf{f}}_\omega^\dagger(\mathbf{r}) \cdot \hat{\mathbf{f}}_\omega(\mathbf{r})$$

$$- \sum_{i=1,2}\left[\hat{\sigma}_{i0}\int_0^{+\infty} d\omega \mathbf{d}_{i0} \cdot \hat{\mathbf{E}}_\omega^+(\mathbf{r}_d) + \text{H.c.}\right], \quad (1)$$

where the atomic operator $\hat{\sigma}_{ii} = |i\rangle\langle i|$ with $|i\rangle(i = 1, 2)$ being the two excited states of QE located at $\mathbf{r}_d$. $\hat{\mathbf{f}}_\omega$ is the bosonic annihilation for the electric field of MoS$_2$ nanodisk, which is represented by a continuum of harmonic oscillators. In (1), the first term stands for the energy of the V-type QE and the decay rate γ_0 of the two excited states. The second term refers to the energy of vacuum electromagnetic field, and the last term describes the QE-electromagnetic field interaction, where the electric field operator $\hat{\mathbf{E}}_\omega^+(\mathbf{r}_d)$ is given by

$$\hat{\mathbf{E}}_\omega^+(\mathbf{r}_d) = i\sqrt{\frac{\hbar}{\pi\varepsilon_0}}\frac{\omega^2}{c^2}\int d\mathbf{r}'\sqrt{\text{Im}[\varepsilon'_\omega(\mathbf{r}')]}\mathbf{G}_\omega(\mathbf{r}_d, \mathbf{r}')\hat{\mathbf{f}}_\omega(\mathbf{r}'), \quad (2)$$

where $\varepsilon'_\omega(\mathbf{r}')$ denotes the complex dielectric function of MoS$_2$ nanodisk. ω is the angular frequency and c denotes the speed of light in the vacuum. $\mathbf{G}_\omega(\mathbf{r}_d, \mathbf{r}')$ denotes the classical electromagnetic Green's tensor with frequency ω at $\mathbf{r}_d$ and a point source located at $\mathbf{r}'$. Taking into account the electrostatic approximation [20], the total Green's tensor for the MoS$_2$ nanodisk is given as $\mathbf{G}_\omega^{\text{tot}}(\mathbf{r}_d, \mathbf{r}') = \mathbf{G}_\omega^0(\mathbf{r}_d, \mathbf{r}') + \mathbf{G}_\omega^{\text{ind}}(\mathbf{r}_d, \mathbf{r}')$, where $\mathbf{G}_\omega^0(\mathbf{r}_d, \mathbf{r}')$ is the homogeneous part and $\mathbf{G}_\omega^{\text{ind}}(\mathbf{r}_d, \mathbf{r}')$ is the induced part associated with the interaction between the QE and the MoS$_2$ nanodisk.

For studying the spontaneous emission and considering the one-excitation approximation, the wave function of our system

at time t can be written as

$$|\psi(t)\rangle = c_1(t)e^{-i\omega_0 t}|1; \varnothing\rangle + c_2(t)e^{-i\omega_0 t}|2; \varnothing\rangle$$

$$+ \int d\mathbf{r}\int d\omega\mathbf{C}(\mathbf{r}, \omega, t)e^{-i\omega t}|0; 1_{\mathbf{r},\omega}\rangle, \quad (3)$$

where $|n'; a\rangle = |n'\rangle \otimes |a\rangle$, with $|n'\rangle(n' = 0, 1, 2)$ stands for the quantum states of the QE, and $|a\rangle(a = \varnothing, 1_{\mathbf{r},\omega})$ denotes the photon states of the system. $|1; \varnothing\rangle$ ($|2; \varnothing\rangle$) represents that the QE is in the excited state $|1\rangle$ ($|2\rangle$) and there is no photon in the system, while $|0; 1_{\mathbf{r},\omega}\rangle$ indicates that the QE has returned to the ground state and there is one photon in the system with energy $\hbar\omega$. The elementary excitation of the light field is defined through the action of the bosonic vector field operator on the vacuum state $\hat{\mathbf{f}}_\omega^\dagger(\mathbf{r})|\varnothing\rangle = |1_{\mathbf{r},\omega}\rangle$.

A. Induced Electrostatic Green's Tensor

In the following, we develop the effective modes theory based on Green's function to describe the hybrid system. We first give the calculation method of Green's function. In our model, the QE is located at the center of the MoS$_2$ nanodisk, $\mathbf{r}_d = (0, 0, z)$, thus the induced part of the Green's tensor is given by [21], [33]

$$\mathbf{G}_\omega^{xx}(\mathbf{r}_d, \mathbf{r}_d) = -\frac{c^2}{2\omega^2}\sum_{n=0}^\infty c_n^1(z, \omega)\frac{\left[\sqrt{(z/R)^2 + 1} - z/R\right]^{2n+2}}{\sqrt{(z/R)^2 + 1}}, \quad (4)$$

and

$$\mathbf{G}_\omega^{zz}(\mathbf{r}_d, \mathbf{r}_d) = \pm\frac{c^2}{2\omega^2}\sum_{n=1}^\infty c_n^0(z, \omega)\frac{\left[\sqrt{(z/R)^2 + 1} - z/R\right]^{2n+1}}{\sqrt{(z/R)^2 + 1}}, \quad (5)$$

where the minus (plus) sign applies to $z > 0$ ($z < 0$) in (5). The $c_n^l(z, \omega)$ ($l = 0, 1$) represents the expansion coefficients with $l = 0$ and $l = 1$ denoting the dipole moment of the QE are along z- and x-orientations, respectively. In fact, the expansion coefficients $c_n^l(z, \omega)$ form a vector $\mathbf{c}^l = (c_1^l(z, \omega), c_2^l(z, \omega), \ldots, c_n^l(z, \omega))^T$ satisfying the solution of the matrix equation which can be expressed as [19]

$$\left[\Omega_0^2(\omega)\mathbf{K}^l - \omega^2\mathbf{G}^l\right]\mathbf{c}^l = i\frac{\omega\sigma(\omega)}{R^2}\mathbf{D}^l\mathbf{d}^l, \quad (6)$$

where $\Omega_0^2(\omega) = -i\omega\sigma_{\text{MoS}_2}(\omega)/2\epsilon_0 R$ with $\sigma_{\text{MoS}_2}(\omega)$ given in (12). The matrices $\mathbf{D}^l$, $\mathbf{G}^l$ and $\mathbf{K}^l$ have the form:

$$D_{qk}^l = \frac{\delta_{qk}}{2(1 + 2q + 1)}, \quad (7)$$

$$G_{qk}^l = \frac{\delta_{q0}\delta_{k0}}{8l(l+1)^2} + \frac{1}{8}\frac{1}{(l+2q+3)(l+2q+2)(l+2q+1)}\delta_{q+1,k}$$

$$+ \frac{1}{4}\frac{1}{(l+2q+2)(l+2q+1)(l+2q)}\delta_{qk}$$

$$+ \frac{1}{8}\frac{1}{(l+2k+3)(l+2k+2)(l+2k+1)}\delta_{q,k+1}, \quad (8)$$

$$K_{qk}^l = \frac{(-1)^{k-q+1}}{\pi\left[4(k-q)^2-1\right](l+k+q+1/2)(l+k+q+3/2)},$$
$$(9)$$

where $q, k = 1, 2, 3\ldots$ for $l = 0$ and $q, k = 0, 1, 2\ldots$ for $l = 1$. Then, d_k^l are the components of the vector $\mathbf{d}^l$, which are given by

$$d_k^1 = (2k+2)\frac{1}{R^2}\int_0^1 dr P_k^{(1,0)}\left(1-2r^2\right)\frac{r^3}{\left[r^2+(z/R)^2\right]^{3/2}},$$
$$(10)$$

$$d_k^0 = 2(2k+1)\frac{z}{R^3}\int_0^1 dr P_k^{(0,0)}\left(1-2r^2\right)\frac{r}{\left[r^2+(z/R)^2\right]^{3/2}},$$
$$(11)$$

where $P_k^{(l,0)}$ is the Jacobi polynomials.

B. MoS$_2$ Conductivity

From $\Omega_0^2(\omega)$, it can be seen that in order to obtain the Green's function we need to acquire the MoS$_2$ conductivity. The optical response of the MoS$_2$ nanodisk is described through its surface conductivity, called σ_{MoS_2}. Taking into account the interaction of light with the lowest energy A and B excitons [34], the MoS$_2$ nanodisk surface conductivity is given by [22]

$$\sigma_{\text{MoS}_2} = \frac{4\alpha_0 c v^2}{\pi a_{ex}^2 \omega}\sum_{k=A,B}\frac{-i}{E_k - \hbar\omega - i\hbar\gamma_k}.$$
$$(12)$$

where α_0 is the fine structure constant; $a_{ex} = 0.8$ nm stands for the exciton Bohr radius. $\hbar\gamma_A$ and $\hbar\gamma_B$ are the damping parameters with $\hbar\gamma_A = 0.5$ meV and $\hbar\gamma_B = 1.1$ meV; $E_A = 1.9$ eV and $E_B = 2.1$ eV are the exciton energies. Also, v stands for a velocity parameter, and we use $v = 0.55$ nm/fs [35], [36].

C. Localized Exciton Mode Quantization and Effective Model

The photonic density of states of MoS$_2$ nanodisk presents multi-resonance [34] as Fig. 2 shows. Accordingly, we propose an effective multi-mode model to study the quantum dynamics of strong light-matter interaction between the QE and the MoS$_2$ nanodisk [37], [38]. The coupled QE-MoS$_2$ nanodisk system can be described as a V-type QE coupled to N localized exciton (LE) modes supported by the MoS$_2$ nanodisk [23] with different coupling strength, while there is no interaction between the LE modes. Therefore, the effective Hamiltonian of hybrid system takes the same form as multi-mode Jaynes–Cummings model, which is given in (13), shown at the bottom of this page.

The $\hat{\sigma}_+^{(1)} = |1\rangle\langle 0|$ is the raising operator of excited state $|1\rangle$, with the transition electric dipole moments $\mathbf{d}_{10}$. $\hat{\sigma}_+^{(2)} = |2\rangle\langle 0|$
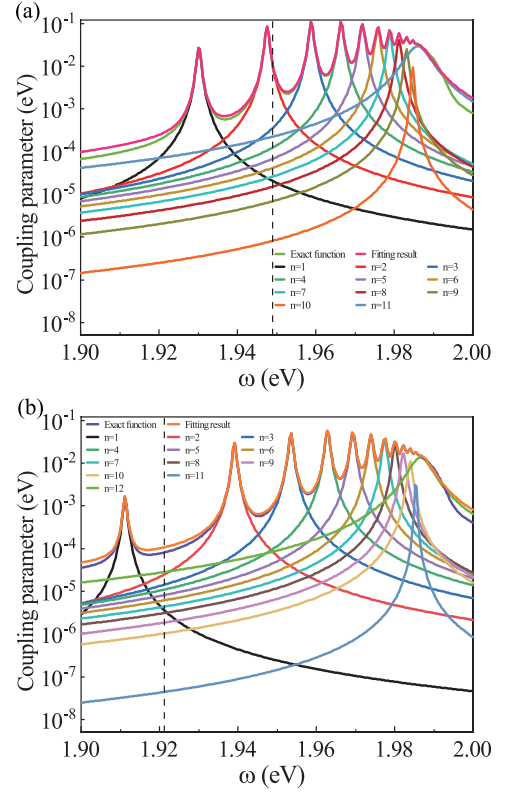

Fig. 2. Comparison of the exact and the fitting photonic density of states $\kappa(\omega)$ for a V-type QE located 2 nm away from a MoS$_2$ nanodisk of radius $R = 30$ nm. Each coupling parameter $g_n(\omega)$ is also plotted. (a) The multi-Lorentzian model used for fitting covers all the LE$_n$ mode for $\mu_{21}^{(\bar{n})} = 1$. The vertical black and dashed lines correspond to the QE $\omega_0 = 1.94892$ eV for $\mu_{21}^{(\bar{n})} = 1$. (b) Same as (a) but for $\mu_{21}^{(\bar{n})} = -1$, The vertical black and dashed lines correspond to the QE with $\omega_0 = 1.92128$ eV for $\mu_{21}^{(\bar{n})} = -1$.

is the raising operator of excited state $|2\rangle$, with the transition electric dipole moments $\mathbf{d}_{20}$. $\bar{n}$ is compact index notation, which can be interpreted as a spatial coordinate under a column coordinate system description. $\hat{b}_{\bar{n}}^{(1)}$ and $\hat{b}_{\bar{n}}^{(2)}$ are the two new bosonic field operators of LE$_{\bar{n}}$ mode ($\bar{n}$-th LE mode) of MoS$_2$ nanodisk, as a function of the coupling between the field and excited states $|1\rangle, |2\rangle$ of the V-type QE, respectively [39]. $\omega_{\bar{n}}$ and $\gamma_{\bar{n}}$ are the corresponding resonance frequency and decay rate, respectively. $\tilde{g}_{\bar{n}}^{(ji)}(j = 1, 2; i = 1, 2)$ is the coupling strength for the interaction between the excited state $|i\rangle$ of QE and the electric field of LE$_{\bar{n}}$ mode. The specific expressions of $\tilde{g}_{\bar{n}}^{(ji)}$ are given by

$$\tilde{g}_{\bar{n}}^{(11)} = g_{\bar{n}}^{(1)},\tag{14}$$

$$\tilde{g}_{\bar{n}}^{(12)} = \mu_{21}^{(\bar{n})}g_{\bar{n}}^{(2)},\tag{15}$$

$$\hat{H}_{\text{eff}} = \hbar\left(\omega_0 - i\frac{\gamma_0}{2}\right)(\hat{\sigma}_{11} + \hat{\sigma}_{22}) + \sum_{\bar{n}}\hbar\left(\omega_{\bar{n}} - i\frac{\gamma_{\bar{n}}}{2}\right)\left(\hat{b}_{\bar{n}}^{(1)\dagger}\hat{b}_{\bar{n}}^{(1)} + \hat{b}_{\bar{n}}^{(2)\dagger}\hat{b}_{\bar{n}}^{(2)}\right)$$

$$- i\hbar\sum_{\bar{n}}\left(\tilde{g}_{\bar{n}}^{(11)}\hat{b}_{\bar{n}}^{(1)}\hat{\sigma}_+^{(1)} + \tilde{g}_{\bar{n}}^{(22)}\hat{b}_{\bar{n}}^{(2)}\hat{\sigma}_+^{(2)} + \tilde{g}_{\bar{n}}^{(12)}\hat{b}_{\bar{n}}^{(1)}\hat{\sigma}_+^{(2)} + \tilde{g}_{\bar{n}}^{(21)}\hat{b}_{\bar{n}}^{(2)}\hat{\sigma}_+^{(1)} - \mathbf{H.c.}\right).\tag{13}$$

$$\tilde{g}_{\bar{n}}^{(22)} = \sqrt{1 - \left|\mu_{\bar{n}}^{(21)}\right|^2}\, g_{\bar{n}}^{(2)}, \tag{16}$$

$$\tilde{g}_{\bar{n}}^{(21)} = 0, \tag{17}$$

where $g_{\bar{n}}^{(1)}$ and $g_{\bar{n}}^{(2)}$ are the coupling strength for the interaction between the excited states $|1\rangle$, $|2\rangle$ of the QE and the electric field of $LE_{\bar{n}}$ mode when the excited states $|1\rangle$, $|2\rangle$ are assumed to exist individually, respectively. $\mu_{21}^{(\bar{n})}$ stands for the mode overlap and is given by

$$\mu_{21}^{(\bar{n})} = (-1)^l. \tag{18}$$

For nanodisk structures, the plasmon eigenmodes can be classified by angular momentum l and contain a subset of radial indexes n to describe the various types of modes in radial constraints [40], which we can obtain $\bar{n} = (l, n)$. For the hybrid systems studied in this paper, the mode overlap takes a value of either $\mu_{21}^{(\bar{n})} = 1$ or $\mu_{21}^{(\bar{n})} = -1$, corresponding to when the angular momentum is $l = 0$ or $l = 1$ in our model, respectively. Now, we can take n instead of the compact index $\bar{n}$ under the condition that $\mu_{21}^{(\bar{n})} = 1$ or $\mu_{21}^{(\bar{n})} = -1$.

Therefore, we can express the effective multi-mode Hamiltonian ((13)) in the matrix form in the basis $\{|1, \varnothing\rangle, |g, 1_1\rangle, \ldots, |g, 1_N\rangle, |2, \varnothing\rangle\}$ [28], [37]

$$\hat{H}_{\text{eff}} =$$

$$\hbar \begin{pmatrix} -i\frac{\gamma_0}{2} & g_1^{(1)} & g_2^{(1)} & \cdots & g_N^{(1)} & 0 \\ g_1^{(1)} & \triangle_1 - i\frac{\gamma_1}{2} & 0 & \cdots & 0 & g_1^{(2)} \\ g_2^{(1)} & 0 & \triangle_2 - i\frac{\gamma_2}{2} & \ddots & \vdots & g_2^{(2)} \\ \vdots & \vdots & \ddots & \ddots & 0 & \vdots \\ g_N^{(1)} & 0 & 0 & \cdots & \triangle_n - i\frac{\gamma_N}{2} & g_N^{(2)} \\ 0 & g_1^{(2)} & g_2^{(2)} & \cdots & g_N^{(2)} & -i\frac{\gamma_0}{2} \end{pmatrix}, \tag{19}$$

where $\triangle_n = \omega_n - \omega_0$ is the detuning between the LE_n mode and the QE.

III. RESULTS AND DISCUSSION

In this section, we discuss the population dynamics of the coupled system. We first find and determine all the frequencies of plasmonic resonance in MoS_2 nanodisks. Then we use a multi-Lorentzian model to derive the coupling strength g_n for each LE_n mode. Finally, we present the results for the excited states of the V-type QE and partial LE_n modes for two initial states and various transition frequency.

The MoS_2 nanodisk supports LE modes at the resonance frequencies ω_n^l obtained by numerically solving the equation

$$\sigma_{\text{MoS}_2}(\omega_n^l)/\omega_n^l = 2i\varepsilon_0 R/\zeta_n^l, \tag{20}$$

where ζ_n^l denotes the disk geometry eigenmodes which correspond to the plasmon resonances in individual 2D nanodisk [19], [41]. The ζ_n^l is obtained numerically by solving the equation

TABLE I
PARAMETERS OF MULTI-LORENTZIAN MODEL

	$\mu_{21}^{(\bar{n})} = 1$			$\mu_{21}^{(\bar{n})} = -1$		
n	ω_n(eV)	g_n(eV)	γ_n(eV)	ω_n(eV)	g_n(eV)	γ_n(eV)
1	1.93017	0.00678	0.000499	1.91119	0.001542	0.000477
2	1.94758	0.01176	0.000532	1.93914	0.006956	0.000515
3	1.95885	0.01387	0.000566	1.95353	0.009204	0.000550
4	1.96648	0.01419	0.000594	1.96289	0.010126	0.000582
5	1.97187	0.01350	0.000614	1.96933	0.009865	0.000607
6	1.97585	0.01226	0.000627	1.97396	0.009231	0.000627
7	1.97887	0.01075	0.000631	1.97743	0.008235	0.000638
8	1.98125	0.00896	0.000617	1.98011	0.007210	0.000646
9	1.98316	0.00669	0.000564	1.98244	0.005897	0.000621
10	1.98472	0.00316	0.000327	1.98397	0.004578	0.000608
11	1.98602	0.01728	0.003245	1.98539	0.001958	0.000148
12				1.98659	0.011246	0.002991

which is give by

$$\mathbf{K}^l \mathbf{c}_n^l = \zeta_n^l \mathbf{G}^l \mathbf{c}_n^l. \tag{21}$$

To determine the coupling strength g_n for each LE_n mode, we introduce a multi-Lorentzian model for the photonic density of states [30]

$$\kappa(\omega) \equiv \sum_n |g_n(\omega)|^2 = \frac{\omega^2}{\hbar\pi\varepsilon_0 c^2} \mathbf{d} \cdot \text{Im}\left[\mathbf{G}\left(\mathbf{r}_d, \mathbf{r}_d, \omega\right)\right] \cdot \mathbf{d}^*, \tag{22}$$

where $g_n(\omega) = \sqrt{\frac{\gamma_n}{2\pi}} \frac{g_n(\mathbf{r}_d)}{\omega - \omega_n + i\frac{\gamma_n}{2}}$ is the coupling parameter. ω_n can be obtained from the (20) depending on the vaule of $\mu_{21}^{(\bar{n})}$. According to the dipole moment of the V-type QE and the (22), it can be seen that $g_n^{(1)}$ is equal to $g_n^{(2)}$. Thus, we can evaluate the values of coupling strength and decay rate through $\mathbf{d} = \mathbf{d}_{20}$. The mode overlap takes the value as $\mu_{21}^{(\bar{n})} = -1$ corresponding to $\sum_n |g_n(\omega)|^2 = \frac{\omega^2}{\hbar\varepsilon_0 c^2} \mathbf{d}_{20} \cdot \text{Im}[\mathbf{G}_\omega^{xx}(\mathbf{r}_d, \mathbf{r}_d)] \cdot \mathbf{d}_{20}^*$, and the mode overlap takes the value as $\mu_{21}^{(\bar{n})} = 1$ corresponding to $\sum_n |g_n(\omega)|^2 = \frac{\omega^2}{\hbar\varepsilon_0 c^2} \mathbf{d}_{20} \cdot \text{Im}[\mathbf{G}_\omega^{zz}(\mathbf{r}_d, \mathbf{r}_d)] \cdot \mathbf{d}_{20}^*$.

We consider a dipole moment of $d = 24\,\text{D}$ of the V-type QE placed at $\mathbf{r}_d = (0, 0, 2\,\text{nm})$ from the MoS_2 nanodisk with radius $R = 30\,\text{nm}$, and then we can obtain the parameters of the multi-Lorentzian model by simple curve fitting. The obtained parameters are listed in Tabel 1, the fitting results are presented in Fig. 2.

Finally, we discuss the population dynamics for the excited states of the V-type QE and partial LE_n modes. In the following study, we consider that the QE excited states have a decay rate of $\gamma_0 = 0.05\,\text{meV}$ [21]. For the effective Hamiltonian (19), we define the right and left eigenvectors $|\Pi_m^R\rangle$ and $|\Pi_m^L\rangle$, respectively, with $\hat{H}_{\text{eff}}|\Pi_m^R\rangle = \lambda_m|\Pi_m^R\rangle$ and $\hat{H}_{\text{eff}}^\dagger|\Pi_m^L\rangle = \lambda_m^*|\Pi_m^L\rangle$. The eigenvectors satisfy the relation $\langle\Pi_m^L|\Pi_n^R\rangle = \delta_{mn}$. The eigenvectors can be written as [42]

$$\left|\Pi_m^R\right\rangle = m_{01}|1\rangle|\varnothing\rangle + \sum_{n=1}^N m_n|g\rangle|1_n\rangle + m_{02}|2\rangle|\varnothing\rangle, \tag{23}$$

$$\left|\Pi_m^L\right\rangle = -m_{01}^\star|1\rangle|\varnothing\rangle + \sum_{n=1}^N m_n^*|g\rangle|1_n\rangle - m_{02}^\star|2\rangle|\varnothing\rangle, \tag{24}$$
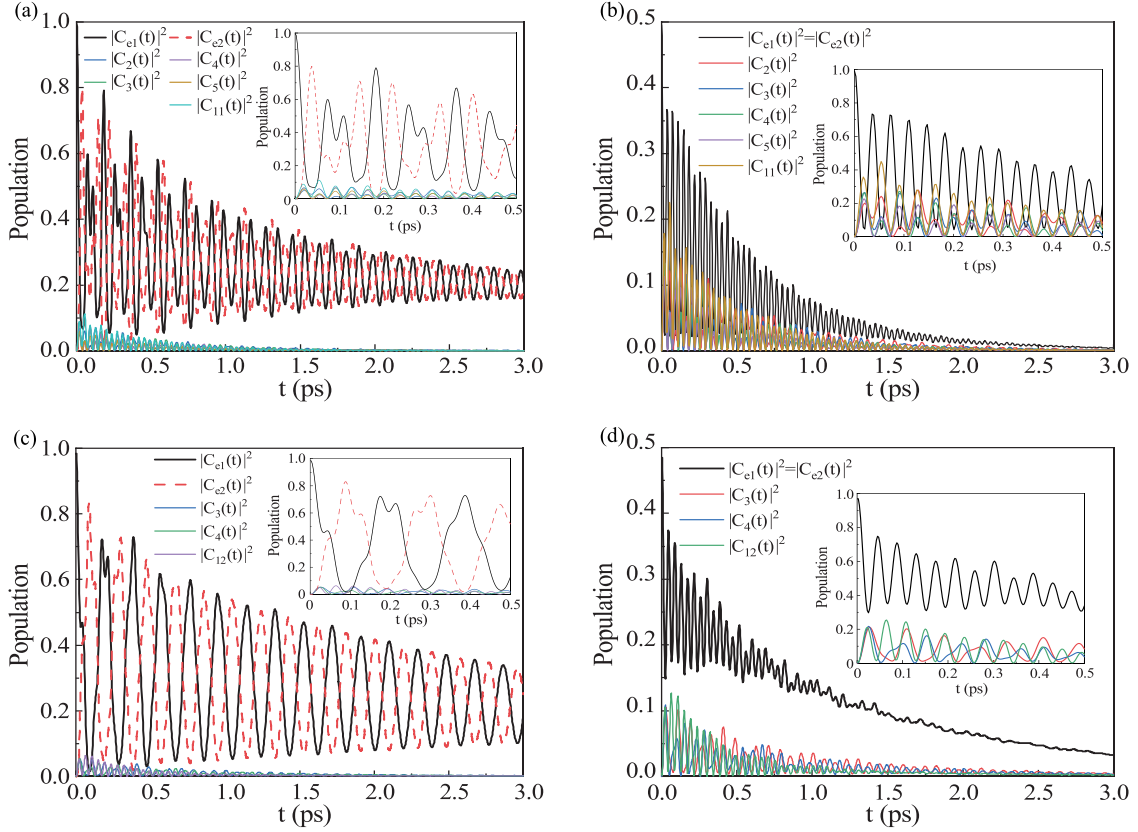
Fig. 3. The population dynamics of the excited states of QE and the partial LE_n modes with high population. (a) $\mu_{21}^{(n)} = 1$, $\omega_0 = 1.94892\,\text{eV}$, with the initial state $|\psi_{\text{eff}}(0)\rangle = |1\rangle|\varnothing\rangle$. (b) Same as (a) but for initial state $|\psi_{\text{eff}}(0)\rangle = \sqrt{\frac{1}{2}}|1\rangle|\varnothing\rangle + \sqrt{\frac{1}{2}}|2\rangle|\varnothing\rangle$. (c) $\mu_{21}^{(n)} = -1$, $\omega_0 = 1.92128\,\text{eV}$, with the initial state $|\psi_{\text{eff}}(0)\rangle = |1\rangle|\varnothing\rangle$. (d) Same as (c) while the initial state is $|\psi_{\text{eff}}(0)\rangle = \sqrt{\frac{1}{2}}|1\rangle|\varnothing\rangle + \sqrt{\frac{1}{2}}|2\rangle|\varnothing\rangle$. The inset shows the same dynamics as the main panel but for $t < 0.5\,\text{ps}$. In all figures, the QE with decay rate $\gamma_0 = 0.05\,\text{meV}$ is located 2 nm away from a MoS₂ nanodisk of radius $R = 30\,\text{nm}$.

where the expansion coefficients m_{01}, $m_n(n = 1, 2, \ldots, N)$ and m_{02} are the values of the elements of the normalized eigenvector $|\Pi_m^R\rangle$ in the basis $\{|1, \varnothing\rangle, |g, 1_1\rangle, \ldots, |g, 1_N\rangle, |2, \varnothing\rangle\}^T$, which are also called the Hopfield coefficients [43], [44]. Accordingly, the wavefunction of at time t is written as

$$|\psi_{\text{eff}}(t)\rangle = C_{e1}(t)|1\rangle|\varnothing\rangle + C_{e2}(t)|2\rangle|\varnothing\rangle + \sum_{n=1}^{N} C_n(t) \cdot |g\rangle|1_n\rangle$$

$$= \sum_{m=1}^{N+2} \eta_m |\Pi_m^R\rangle e^{-i\lambda_m t}. \tag{25}$$

The estimation of the coefficient η_m depends on the initial state of the system. We consider two initial states, $|\psi_{\text{eff}}(0)\rangle = |1\rangle|\varnothing\rangle$ for QE excited state $|1\rangle$ and the superposition state $|\psi_{\text{eff}}(0)\rangle = \sqrt{\frac{1}{2}}|1\rangle|\varnothing\rangle + \sqrt{\frac{1}{2}}|2\rangle|\varnothing\rangle$. For the former case, the coefficient η_m is expressed as $\eta_m = \langle \Pi_m^L \mid \psi_{\text{eff}}(0)\rangle = -m_{01}$, and the wavefunction is written as $|\psi_{\text{eff}}(t)\rangle = \sum_{m=1}^{N+2} \eta_m |\Pi_m^R\rangle e^{-i\lambda_m t} = \sum_{m=1}^{N+2} -m_{01}|\Pi_m^R\rangle e^{-i\lambda_m t}$. The time evolution of the excited state $|1\rangle$ and $|2\rangle$ are given by $|C_{e1}(t)|^2 = |\langle 1, \varnothing|\psi_{\text{eff}}(t)\rangle|^2 = |\sum_{m=1}^{N+2} m_{01}^2 e^{-i\lambda_m t}|^2$ and $|C_{e2}(t)|^2 = |\langle 2, \varnothing|\psi_{\text{eff}}(t)\rangle|^2 = |\sum_{m=1}^{N+2} m_{01}m_{02}e^{-i\lambda_m t}|^2$, respectively. On the other hand, the population of nth

LE mode is expressed as $|C_n(t)|^2 = |\langle 0, 1_n|\psi_{\text{eff}}(t)\rangle|^2 = |\sum_{m=1}^{N+2} m_{01}m_n e^{-i\lambda_m t}|^2$, where λ_m denotes the eigenvalue of the effective Hamiltonian, which is given by

$$\lambda_m = \omega_m - i\frac{\gamma_m}{2}, \tag{26}$$

where we take $m = 1, \ldots, N + 2$ for LE modes $N = 11$ and 2.

While for the case of superposition state as the initial state, we obtain the coefficient $\eta_m = \langle \Pi_m^L \mid \psi_{\text{eff}}(0)\rangle = -\sqrt{\frac{1}{2}}m_{01} - \sqrt{\frac{1}{2}}m_{02}$, and the wavefunction is expressed as $|\psi_{\text{eff}}(t)\rangle = \sum_{m=1}^{N+2} \eta_m |\Pi_m^R\rangle e^{-i\lambda_m t} = \sum_{m=1}^{N+2} \left(-\sqrt{\frac{1}{2}}m_{01} - \sqrt{\frac{1}{2}}m_{02}\right)|\Pi_m^R\rangle e^{-i\lambda_m t}$. We can obtain the time evolution of the excited states $|1\rangle$ and $|2\rangle$ as $|C_{e1}(t)|^2 = |\langle 1, \varnothing|\psi_{\text{eff}}(t)\rangle|^2 = \frac{1}{2}|\sum_{m=1}^{N+2}(m_{01} + m_{02})m_{01}e^{-i\lambda_m t}|^2$ and $|C_{e2}(t)|^2 = |\langle 2, \varnothing|\psi_{\text{eff}}(t)\rangle|^2 = \frac{1}{2}|\sum_{m=1}^{N+2}(m_{01} + m_{02})m_{02}e^{-i\lambda_m t}|^2$, respectively. While the population of LE_n modes is $|C_n(t)|^2 = |\langle 0, 1_n|\psi_{\text{eff}}(t)\rangle|^2 = \frac{1}{2}|\sum_{m=1}^{N+2}(m_{01} + m_{02})m_n e^{-i\lambda_m t}|^2$.

In Fig. 3, we present the population dynamics of a V-type QE and LE with transition frequency $\omega_0 = 1.94892\,\text{eV}$[21]. The population evolution of $|C_{e1}(t)|^2$, $|C_{e2}(t)|^2$ and partial LE_n modes for initial state $|\psi_{\text{eff}}(0)\rangle = |1\rangle|\varnothing\rangle$ are shown in

Fig. 3(a) for time $t < 3$ ps. The population dynamics exhibits evident oscillation, a strong characteristic of non-Markovian dynamics. It can be seen that the population of the initial state $|\psi_{\text{eff}}(0)\rangle = |1\rangle|\varnothing\rangle$ decays rapidly within about 50 fs. Specifically, we observe that the oscillation of population transfers between the excited states $|1\rangle$ and $|2\rangle$, indicating that the V-type QE couples to LE_n modes supported by the MoS_2 nanodisk. The excited states population of the V-type QE decays to about 20% of its initial value within the first 3 ps and remains a period of time. Furthermore, we find that the LE_2, LE_4 and LE_{11} modes primarily govern the population transfer between the states of the QE and the nanodisk. The inset in Fig. 3(a) shows that the effective mode have the same oscillation period as the excited state population of the QE. We thus observe the multiple channels energy transfer process. The energy transfer direction are from initial state $|1\rangle$ to effective modes (LE_2, LE_3, LE_4, LE_5 and LE_{11}), and then from LE effective modes to QE states $|1\rangle$ and $|2\rangle$.

In Fig. 3(b), the time evolution of $|C_{e1}(t)|^2$, $|C_{e2}(t)|^2$, and partial LE_n modes with initial state $|\psi_{\text{eff}}(0)\rangle = \sqrt{\frac{1}{2}}|1\rangle|\varnothing\rangle + \sqrt{\frac{1}{2}}|2\rangle|\varnothing\rangle$ are shown during the first 3 ps. It can be seen that the evolution of $|C_{e1}(t)|^2$ is equal to $|C_{e2}(t)|^2$ at any time. We note that the population of the V-type QE states $|1\rangle$ and $|2\rangle$ decays totally within about 3 ps. Moreover, we observe that the energy transfer between the QE and nanodisk mainly occurs in the LE_2, LE_3, LE_4, LE_5 and LE_{11} modes. Compared to Fig. 3(a), there are more effective modes taking the lead in the energy transfer process. Under with initial state $|\psi_{\text{eff}}(0)\rangle = \sqrt{\frac{1}{2}}|1\rangle|\varnothing\rangle + \sqrt{\frac{1}{2}}|2\rangle|\varnothing\rangle$, the population dynamics of the QE and effective modes exhibits the characteristic of higher-frequency oscillation. In addition, the channel of the energy transfer is either from the two upper states of the QE to effective modes or the reversible process as shown in the inset of Fig. 3(b).

Lastly, we consider the case of the V-type QE with transition frequency $\omega_0 = 1.92128$ eV [21]. The population dynamics of a V-type QE and LE is presented in Fig. 3(c) and (d). Under these conditions, we obtain $N = 12$ from (22) and numerically time evolution $|C_{e1}(t)|^2$, $|C_{e2}(t)|^2$ and $|C_n(t)|^2$. In Fig. 3(c), we show the population evolution $|C_{e1}(t)|^2$, $|C_{e2}(t)|^2$, and partial LE_n modes with initial state $|\psi_{\text{eff}}(0)\rangle = |1\rangle|\varnothing\rangle$ during the first 3 ps. The strong non-Markovian character can be observed in the inset of Fig. 3(c). We find that the oscillation of population transfer between states $|1\rangle$ and $|2\rangle$ decreases over time. The result indicates that the V-type QE interacts with the nth mode. The excited states population of the V-type QE decays to about 30% of its initial value within the first 3 ps. Furthermore, we notice that the energy transfer between the QE and nanodisk mainly occurs in the LE_4 and LE_{12} modes. Compared to Fig. 3(a), we find that the effective modes (LE_3, LE_4, LE_{12}) have a lower amplitude and oscillation frequency, which leads to a smooth change of population during the dynamics of QE at early stage. In addition, the population dynamics of QE exhibits the small oscillation and longer oscillation period during the first 0.5 ps due to the relatively weak coupling to the effective modes.

In Fig. 3(d), we present the time evolution of $|C_{e1}(t)|^2$, $|C_{e2}(t)|^2$, and partial LE_n modes with initial state $|\psi_{\text{eff}}(0)\rangle = \sqrt{\frac{1}{2}}|1\rangle|\varnothing\rangle + \sqrt{\frac{1}{2}}|2\rangle|\varnothing\rangle$ during the first 3 ps. We also notice the non-Markovian characteristic in the population dynamics of the V-type QE. We note that the population of the V-type QE states $|1\rangle$ and $|2\rangle$ decays rapidly with high-frequency oscillation and completely decreases within about 7 ps (not shown here). Moreover, we notice that the energy transfer between the QE and the nanodisk mainly occurs in the LE_3, LE_4 and LE_{12} modes. In contrast to the results shown in Fig. 3(c), the effective modes (LE_3, LE_4 and LE_{12}) have higher frequency and larger oscillation amplitude, leading to a more rapid decay of QE within the first 3 ps. Furthermore, during the first 3 ps, the QE decay presented in Fig. 3(b) is more drastic compared to Fig. 3(d). The reason is that both the number and oscillation strength involved in the energy transfer from the effective modes to the QE are larger.

IV. CONCLUSION

In conclusion, we study the population dynamics of a QE near a MoS_2 nanodisk with different initial states based on the proposed effective multi-mode model. An effective Hamiltonian for the hybrid system is derived from our model, which is in the same form as the multi-mode Jaynes–Cummings model, and thus corresponding to the conventional cQED description. By quantifying the photonic density of states of MoS_2 nanodisk through a multi-Lorentzian model, we can determine the parameters of the effective Hamiltonian to investigate the quantum dynamics of the system in the manner of cQED. We find that oscillatory population dynamics between the two excited states of the V-type QE, which clearly exhibits the non-Markovian feature. We also find that the energy transfer between the V-type QE and the LE_n modes associated with different initial states. For spontaneous emission process with OE initially in one of the excited state, the resultant decay of QE population is observably slower than that of QE initially in the superposition state since the latter case involves more effective modes that contribute to the coupling of QE to MoS_2 nanodisk and these effective modes have higher frequency and greater oscillation. We believe that the proposed effective multi-mode model can provide insight into the strong light-matter interaction between the QE and the 2D materials and is helpful to develop the advanced quantum technologies.

REFERENCES

[1] P. Törmä and W. L. Barnes, "Strong coupling between surface plasmon polaritons and emitters: A review," *Rep. Prog. Phys.*, vol. 78, no. 1, 2014, Art. no. 013901.

[2] P. Vasa and C. Lienau, "Strong light–matter interaction in quantum emitter/metal hybrid nanostructures," *ACS Photon.*, vol. 5, no. 1, pp. 2–23, 2018.

[3] M. Noginov et al., "Demonstration of a spaser-based nanolaser," *Nature*, vol. 460, no. 7259, pp. 1110–1112, 2009.

[4] M. Premaratne and M. I. Stockman, "Theory and technology of SPASERs," *Adv. Opt. Photon.*, vol. 9, no. 1, pp. 79–128, 2017.

[5] E. I. Galanzha et al., "Spaser as a biological probe," *Nat. Commun.*, vol. 8, no. 1, pp. 1–7, 2017.

[6] N. Kongsuwan et al., "Quantum plasmonic immunoassay sensing," *Nano Lett.*, vol. 19, no. 9, pp. 5853–5861, 2019.

[7] Y. W. Lu, J. F. Liu, R. Liu, R. Su, and X. H. Wang, "Quantum exceptional chamber induced by large nondipole effect of a quantum dot coupled to a nano-plasmonic resonator," *Nanophotonics*, vol. 10, no. 9, pp. 2431–2440, 2021.

[8] R. Chikkaraddy et al., "Single-molecule strong coupling at room temperature in plasmonic nanocavities," *Nature*, vol. 535, no. 7610, pp. 127–130, 2016.

[9] R. Liu et al., "Strong light-matter interactions in single open plasmonic nanocavities at the quantum optics limit," *Phys. Rev. Lett.*, vol. 118, no. 23, 2017, Art. no. 237401.

[10] Q. Zhao et al., "Plexcitonic strong coupling: Unique features, applications, and challenges," *J. Phys. D. Appl. Phys.*, vol. 55, no. 20, 2022, Art. no. 203002.

[11] J. Hakami, L. Wang, and M. S. Zubairy, "Spectral properties of a strongly coupled quantum-dot–metal-nanoparticle system," *Phys. Rev. A*, vol. 89, no. 5, 2014, Art. no. 053835.

[12] I. Thanopulos, V. Yannopapas, and E. Paspalakis, "Non-Markovian dynamics in plasmon-induced spontaneous emission interference," *Phys. Rev. B*, vol. 95, no. 7, 2017, Art. no. 075412.

[13] N. Iliopoulos, I. Thanopulos, V. Yannopapas, and E. Paspalakis, "Counter-rotating effects and entanglement dynamics in strongly coupled quantum-emitter–metallic-nanoparticle structures," *Phys. Rev. B*, vol. 97, no. 11, 2018, Art. no. 115402.

[14] P. Anger, P. Bharadwaj, and L. Novotny, "Enhancement and quenching of single-molecule fluorescence," *Phys. Rev. Lett.*, vol. 96, no. 11, 2006, Art. no. 113002.

[15] C. Van Vlack, P. T. Kristensen, and S. Hughes, "Spontaneous emission spectra and quantum light-matter interactions from a strongly coupled quantum dot metal-nanoparticle system," *Phys. Rev. B*, vol. 85, no. 7, 2012, Art. no. 075303.

[16] M. Antón et al., "Plasmonic effects in excitonic population transfer in a driven semiconductor–metal nanoparticle hybrid system," *Phys. Rev. B*, vol. 86, no. 15, 2012, Art. no. 155305.

[17] S. Kühn, U. Håkanson, L. Rogobete, and V. Sandoghdar, "Enhancement of single-molecule fluorescence using a gold nanoparticle as an optical nanoantenna," *Phys. Rev. Lett.*, vol. 97, no. 1, 2006, Art. no. 017402.

[18] A. Kumar, K. H. Fung, M. H. Reid, and N. X. Fang, "Photon emission rate engineering using graphene nanodisc cavities," *Opt. Exp.*, vol. 22, no. 6, pp. 6400–6415, 2014.

[19] V. D. Karanikolas, C. A. Marocico, and A. L. Bradley, "Tunable and long-range energy transfer efficiency through a graphene nanodisk," *Phys. Rev. B*, vol. 93, no. 3, 2016, Art. no. 035426.

[20] I. Thanopulos, V. Karanikolas, and E. Paspalakis, "Spontaneous emission of a quantum emitter near a graphene nanodisk under strong light-matter coupling," *Phys. Rev. A*, vol. 106, no. 1, 2022, Art. no. 013718.

[21] N. Iliopoulos, V. Karanikolas, I. Thanopulos, and E. Paspalakis, "Entanglement dynamics for quantum emitters strongly coupled with molybdenum disulfide nanodisks," *Physica E*, vol. 119, 2020, Art. no. 113967.

[22] I. Thanopulos, K. Blekos, P. Kalozoumis, V. Karanikolas, and E. Paspalakis, "Memory effects and quantum speedup for a quantum emitter near a molybdenum disulfide nanodisk," *Physica E. Low Dimens. Syst. Nanostructures*, vol. 133, 2021, Art. no. 114780.

[23] V. D. Karanikolas and E. Paspalakis, "Localized exciton modes and high quantum efficiency of a quantum emitter close to a MoS$_2$ nanodisk," *Phys. Rev. B*, vol. 96, no. 4, 2017, Art. no. 041404.

[24] I. Thanopulos, V. Karanikolas, and E. Paspalakis, "Non-Markovian spontaneous emission interference near a MoS$_2$ nanodisk," *Opt. Lett.*, vol. 44, no. 14, pp. 3510–3513, 2019.

[25] A. Reserbat-Plantey et al., "Quantum nanophotonics in two-dimensional materials," *ACS Photon.*, vol. 8, no. 1, pp. 85–101, 2021.

[26] H. Jiao et al., "HgCdTe/black phosphorus van der Waals hetero- junction for high-performance polarization-sensitive midwave infrared photodetector," *Sci. Adv.*, vol. 8, no. 19, 2022, Art. no. eabn1811.

[27] L. Tong et al., "2D materials–based homogeneous transistor- memory architecture for neuromorphic hardware," *Science*, vol. 373, no. 6561, pp. 1353–1358, 2021.

[28] H. Varguet, B. Rousseaux, D. Dzsotjan, H. Jauslin, S. Guérin, and G. C. Des Francs, "Non-Hermitian Hamiltonian description for quantum plasmonics: From dissipative dressed atom picture to Fano states," *J. Phys. B*, vol. 52, no. 5, 2019, Art. no. 055404.

[29] H. Varguet, B. Rousseaux, D. Dzsotjan, H. Jauslin, S. Guérin, and G. C. des Francs, "Dressed states of a quantum emitter strongly coupled to a metal nanoparticle," *Opt. Lett.*, vol. 41, no. 19, pp. 4480–4483, 2016.

[30] S. Hughes, M. Richter, and A. Knorr, "Quantized pseudomodes for plasmonic cavity QED," *Opt. Lett.*, vol. 43, no. 8, pp. 1834–1837, 2018.

[31] H. Varguet, A. Díaz-Valles, S. Guérin, H. Jauslin, and G Colas des Francs, "Collective strong coupling in a plasmonic nanocavity," *J. Chem. Phys.*, vol. 154, no. 8, 2021, Art. no. 084303.

[32] G. X. Li, F. L. Li, and S. Y. Zhu, "Quantum interference between decay channels of a three-level atom in a multilayer dielectric medium," *Phys. Rev. A*, vol. 64, no. 1, 2001, Art. no. 013819.

[33] A. L. Fetter, "Magnetoplasmons in a two-dimensional electron fluid: Disk geometry," *Phys. Rev. B*, vol. 33, no. 8, pp. 5221–5227, 1986.

[34] V. D. Karanikolas, C. A. Marocico, P. R. Eastham, and A. L. Bradley, "Near-field relaxation of a quantum emitter to two-dimensional semiconductors: Surface dissipation and exciton polaritons," *Phys. Rev. B*, vol. 94, no. 19, 2016, Art. no. 195418.

[35] D. Xiao, G. B. Liu, W. Feng, X. Xu, and W. Yao, "Coupled spin and valley physics in monolayers of MoS$_2$ and other group-VI dichalcogenides," *Phys. Rev. Lett.*, vol. 108, no. 19, 2012, Art. no. 196802.

[36] C. Zhang, H. Wang, W. Chan, C. Manolatou, and F. Rana, "Absorption of light by excitons and trions in monolayers of metal dichalcogenide MoS$_2$: Experiments and theory," *Phys. Rev. B*, vol. 89, no. 20, 2014, Art. no. 205436.

[37] B. Rousseaux, D. Dzsotjan, G. C. des Francs, H.-R. Jauslin, C. Couteau, and S. Guerin, "Adiabatic passage mediated by plasmons: A route towards a decoherence-free quantum plasmonic platform," *Phys. Rev. B*, vol. 93, no. 4, 2016, Art. no. 045422.

[38] D. Dzsotjan, B. Rousseaux, H. Jauslin, G. C. des Francs, C. Couteau, and S. Guerin, "Mode-selective quantization and multimodal effective models for spherically layered systems," *Phys. Rev. A*, vol. 94, no. 2, 2016, Art. no. 023818.

[39] B. Rousseaux, "Control for quantum technologies at the nanoscale," Ph.D. dissertation, Université de Bourgogne Franche-Comté, France, 2016.

[40] P. A. D. Gonçalves, "Plasmonics and light–matter interactions in two–dimensional materials and in metal nanostructures: Classical and quantum considerations," Ph.D. dissertation, Tech. Univ. Denmark, Denmark, 2020.

[41] T. Christensen, W. Wang, A. P. Jauho, M. Wubs, and N. A. Mortensen, "Classical and quantum plasmonics in graphene nanodisks: Role of edge states," *Phys. Rev. B*, vol. 90, no. 24, 2014, Art. no. 241414.

[42] G. Dridi, S. Guérin, H. Jauslin, D. Viennot, and G. Jolicard, "Adiabatic approximation for quantum dissipative systems: Formulation, topology, and superadiabatic tracking," *Phys. Rev. A*, vol. 82, no. 2, 2010, Art. no. 022109.

[43] A. Laucht et al., "Mutual coupling of two semiconductor quantum dots via an optical nanocavity," *Phys. Rev. B*, vol. 82, no. 7, 2010, Art. no. 075305.

[44] W. Zhang et al., "Steering room-temperature plexcitonic strong coupling: A diexcitonic perspective," *Nano Lett.*, vol. 21, no. 21, pp. 8979–8986, 2021.